# Controlling a Ball and Wheel System Using Full-State-Feedback Linearization

## A Testbed for Nonlinear Control Design

MING-TZU HO, YI-WEI TU, and HAO-SHUAN LIN

Since control theory is often mathematically abstract, it is sometimes difficult for students to visualize how the concepts are related to practice. Implementation of control schemes in laboratory experiments, however, can help students grasp abstract concepts. Over the past decades, numerous control laboratory experimental setups, such as the inverted pendulum [1], [2], ball and beam [3], and inverted wedge [4], have been developed for control education and research. These setups provide challenging experiments and high-impact visual demonstrations that make them attractive to students. Moreover, because of inherent nonlinearity, instability, and underactuation, these setups can serve as testbeds for research in nonlinear control systems.

In this article, we consider feedback linearization [5]–[7] for nonlinear control design. The idea behind this approach is to find a diffeomorphism and a state-feedback control law that transform the nonlinear system into a linear time-invariant system. The design is then carried out on the linear system using linear control design techniques. Both full-state-feedback linearization and partial-state-feedback linearization can be considered. In full-state-feedback linearization, also called input-state-feedback linearization, the state equations are fully linearized. In partial-state-feedback linearization, also called input-output-feedback linearization, the input-output map of the system is linearized, while the map from the input to the state can be only partially linearized. Feedback linearization has been applied to various real-world problems [8]–[16] as well as laboratory experiments, such as an electromagnetic system [17], an electromechanical system [18], and motors [19]–[24].

In this article, we introduce the ball and wheel system, which is a feedback linearizable electromechanical system consisting of a wheel and a motor. Over the periphery of the wheel, a ball is balanced by controlling the angle of the wheel through the motor. This system is nonlinear and underactuated. Moreover, the equilibrium of this system is open-loop unstable. It is shown in [25] that the ball and wheel system is flat and feedback linearizable, and a nonlinear controller, which is based on the theory of differential flatness, is designed for trajectory planning and tracking. A video showing experimental tracking control of this system is available at [26]. In [27], the nonlinearity of the ball and wheel system is locally bounded by a chosen sector, and an $H_\infty$ PID controller is designed to achieve local asymptotic stability. In this article, we use full-state-feedback linearization to design a stabilizing controller. The control law is implemented on an experimental apparatus through a digital signal processor (DSP). The effectiveness of the controller is verified through simulation and experimental results.

*Digital Object Identifier 10.1109/MCS.2009.934085*

## EXPERIMENTAL APPARATUS

The experimental setup of the ball and wheel system is shown in Figure 1. A schematic overview of the experimental setup is shown in Figure 2. The system consists of a dc motor and a wheel, which is coupled to the dc motor by a hub. The dc motor is rated at 65 W, 30 V, and 4200 rev/min. The rim of the wheel has a groove to prevent the ball, which is made of steel, from slipping out transversely. To measure the position of the ball, a potentiometer-like sensor is utilized. A resistive wire glued to one side of the groove of the wheel and a copper wire glued to the other side are used to form the sensor, with the metallic ball acting as the wiper of the potentiometer. To assess the behavior of this ball-angle sensor quantitatively, the output voltage of the sensor versus

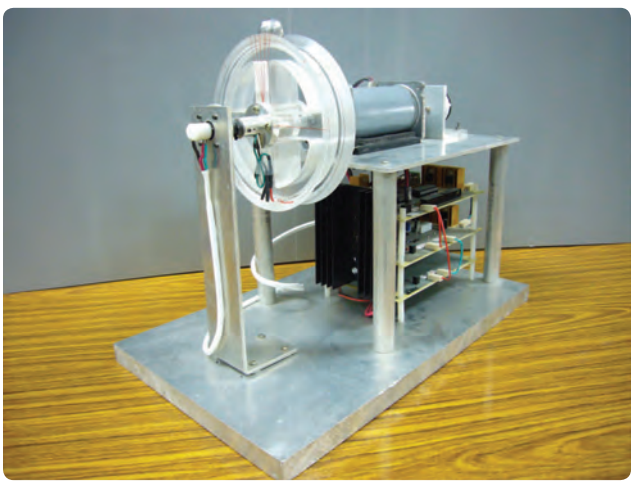

**FIGURE 1** Experimental setup of the ball and wheel system. The wheel is controlled by a dc motor. The objective is to stabilize the ball over the periphery of the wheel at its unstable equilibrium. The system is nonlinear and underactuated.

1066-033X/09/$26.00©2009IEEE

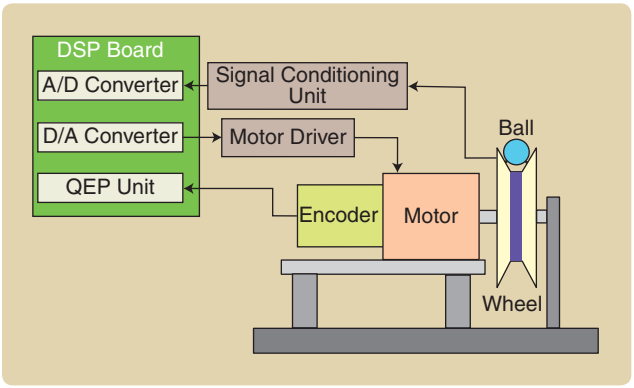


**FIGURE 2** Schematic diagram of the experimental setup. The motor is mounted on an aluminum frame, and the wheel is made from acrylic material. The designed control scheme is implemented on a DSP board equipped with an A/D converter, a D/A converter, and a quadrature encoder pulse unit. The optical encoder measures the angular position of the wheel, while the position of the ball is measured by a potentiometer-like sensor. Through the D/A converter, the control voltage is applied to the motor driver to control the dc motor. The signal conditioning unit amplifies and filters the signal from the ball-angle sensor, and sends the signal to the A/D converter. This system, not including the DSP board, is easy to build and costs about US$200.

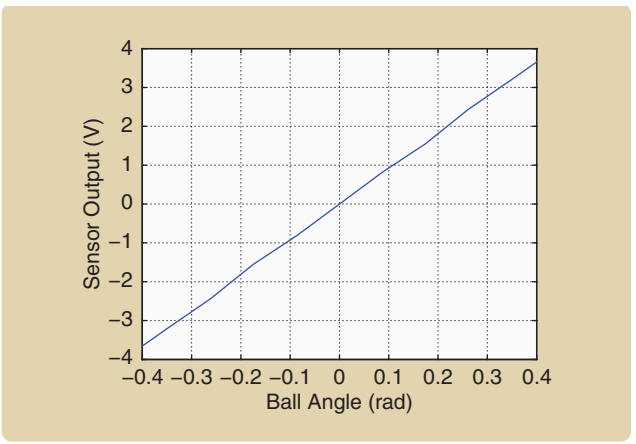


**FIGURE 3** Output voltage of the ball-angle sensor versus the angular position of the ball. To obtain the calibration curve of the sensor, a protractor is used to measure the angular displacement $\theta_1$ of the ball, while the corresponding output voltage is directly read from the voltmeter. Fifteen measurements within the range $[-0.4, 0.4]$ rad are used to plot the calibration curve. This plot shows that the sensor has an approximately linear relation between the output voltage and the angular position of the ball. Using the least-squares method, we obtain the sensitivity of the ball-angle sensor as approximately 9.2 V/rad. Thus, the relation between the measured voltage $v_b$ and the angular displacement $\theta_1$ of the ball is given by $\theta_1\,(\text{rad}) = v_b(\text{V})/9.2(\text{V/rad})$.

the angular position of the ball is plotted in Figure 3, which shows that the angular position of the ball is linearly related to the variation in the output voltage of the sensor. An optical encoder with a resolution of 2000 pulses/rev is attached to the shaft of the dc motor to measure the angular position of the wheel. The encoder produces two quadrature encoder signals and one index signal. The system is controlled by a digital signal processor (150-MHz/32-bit) board equipped with a 12-bit analog-to-digital (A/D) converter, a 12-bit digital-to-analog (D/A) converter, and a quadrature encoder pulse (QEP) unit. The QEP unit provides angular position and rotational direction of the motor from the quadrature encoder signals. The angular velocities of the ball and the wheel are estimated from the angular displacement traveled per unit time and then passed through digital lowpass filters to attenuate the high frequency noise. A voltage signal is generated according to the designed control law and supplied to the power amplifier that drives the dc motor. The power amplifier, which drives the motor in voltage mode, uses an operational amplifier that is set to operate at up to $\pm 20$ V and 2.75 A. In the signal conditioning unit, the signal from the ball-angle sensor is amplified using a low-drift amplifier stage and then passed through an analog anti-aliasing filter. To prevent the wire from tangling due to the rotating wheel, a mercury slip-ring connector is used to transmit the signal from the ball-angle sensor to the signal conditioning unit. The physical parameters of the system are listed in Table 1.

## System Modeling

We derive a mathematical model of the ball and wheel system by using the Euler-Lagrange formulation [28]. Figure 4 illustrates the basic features of the system. Assuming that the coefficient of friction is large enough that the ball rolls on the wheel without slipping, the ball is always in contact with the wires on the wheel. The form of the Euler-Lagrangian equations is

$$\frac{d}{dt}\left[\frac{\partial L}{\partial \dot{q}}\right] - \frac{\partial L}{\partial q} = Q, \tag{1}$$

where $L$ is the Lagrangian function, $Q$ is the generalized forces, and $q$ is the generalized coordinates. The Lagrangian function $L$ is defined as

**TABLE 1 Physical parameters of the system. The mass and geometry are measured. The moment of inertia of the wheel is computed using the dimension, geometry, and mass of the wheel. To estimate the parameters $R_a$ and $K_m$ of the dc motor, a least-squares algorithm is used with samples of the input voltage, output speed, and armature current.**

| Parameter | Value |
|---|---|
| Moment of inertia of the wheel $I_w$ | $1.71 \times 10^{-3}$ kg-m$^2$ |
| Radius of the wheel $r_w$ | 0.075 m |
| Mass of the ball $m_b$ | 0.042 kg |
| Radius of the ball $r_b$ | 0.011 m |
| Motor armature resistance $R_a$ | 0.6558 Ω |
| Motor constant $K_m$ | 0.0662 N-m/A |

$$L = T - V,$$

where $T$ is the kinetic energy and $V$ is the potential energy. For this system, $q$ is selected as

$$q = \begin{bmatrix} \theta_1 \\ \theta_2 \end{bmatrix},$$

where $\theta_1$ is the angular displacement between the $y$ axis and the line through the centers of the ball and the wheel, and $\theta_2$ is the angular displacement of the wheel. $Q$ is given by

$$Q = \begin{bmatrix} 0 \\ \tau \end{bmatrix},$$

where $\tau$ is the torque exerted on the wheel. The kinetic energy of the ball is

$$T_b = \frac{1}{2} m_b (r_w + r_b)^2 \dot{\theta}_1^2 + \frac{1}{2} I_b \dot{\theta}_3^2,$$

where $m_b$ is the mass of the ball, $r_w$ is the radius of the wheel, $r_b$ is the radius of the ball, $\theta_3$ is the angular displacement of the center of the ball relative to the vertical direction, and the moment of inertia of the ball is given by

$$I_b = \frac{2}{5} m_b r_b^2,$$

while the kinetic energy of the wheel is

$$T_w = \frac{1}{2} I_w \dot{\theta}_2^2,$$

where $I_w$ is the moment of inertia of the wheel. Then the total kinetic energy $T$ is

$$\begin{aligned} T &= T_w + T_b \\ &= \frac{1}{2} I_w \dot{\theta}_2^2 + \frac{1}{2} m_b (r_w + r_b)^2 \dot{\theta}_1^2 + \frac{1}{2}\left(\frac{2}{5} m_b r_b^2\right) \dot{\theta}_3^2. \end{aligned}$$

A constraint condition arises as the ball and the wheel rotate and roll over each other. Let $\mathbf{v}_{C_w/O_w}$ denote the velocity of the contact point $C_w$ relative to the center of the wheel $O_w$ and observed from the motor-fixed reference frame as shown in Figure 4. From Figure 4, it follows that

$$\mathbf{v}_{C_w/O_w} = \dot{\theta}_2 r_w \mathbf{e}, \tag{2}$$

where $\mathbf{e}$ is a unit vector that is tangent to the contact point and that points in the direction of increasing $\theta_2$. Also let $\mathbf{v}_{C_b/O_b}$ denote the velocity of the contact point $C_b$ relative to the center of the ball $O_b$ and observed from the motor-fixed reference frame as shown in Figure 4, which is given by

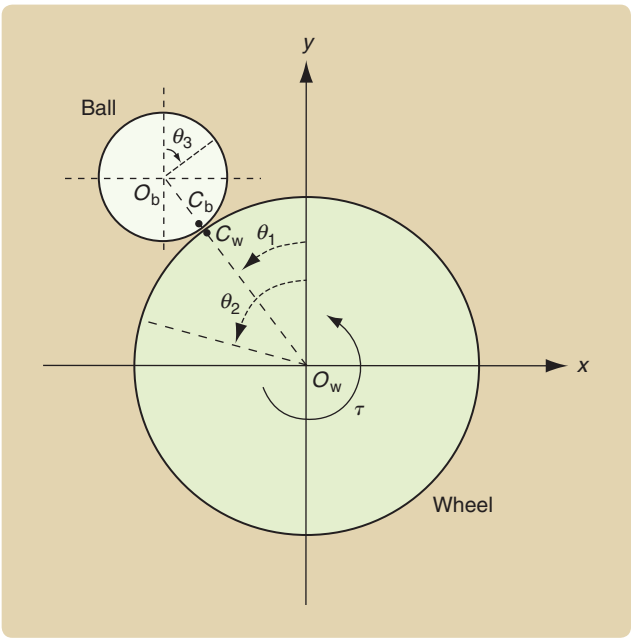


**FIGURE 4** Ball and wheel. Here $\theta_1$ denotes the angular displacement between the $y$ axis and the line through the centers of the ball and the wheel, $\theta_2$ denotes the angular displacement of the wheel, and $\theta_3$ denotes the angular displacement of the ball. $O_b$ and $O_w$ are the centers of the ball and the wheel, respectively. $C_b$ and $C_w$ are the contact points on the ball and the wheel, respectively. $\tau$ is the torque exerted on the wheel. Counterclockwise angles are taken as positive.

$$\mathbf{v}_{C_b/O_b} = \dot{\theta}_3 r_b \mathbf{e}. \tag{3}$$

Under the assumption of rolling without slipping, the contact point $C_b$ is instantaneously at rest relative to the contact point $C_w$ as observed from the motor-fixed reference frame as shown in Figure 4. Hence the velocity of the contact point $C_b$ relative to point $C_w$ is given by

$$\mathbf{v}_{C_b/C_w} = 0. \tag{4}$$

From Figure 4, the velocity of the center of the ball relative to the center of the wheel is

$$\mathbf{v}_{O_b/O_w} = \dot{\theta}_1 (r_w + r_b) \mathbf{e}. \tag{5}$$

From (2)–(4), we obtain

$$\begin{aligned} \mathbf{v}_{O_b/O_w} &= \mathbf{v}_{O_b/C_b} + \mathbf{v}_{C_b/C_w} + \mathbf{v}_{C_w/O_w} \\ &= -\dot{\theta}_3 r_b \mathbf{e} + \dot{\theta}_2 r_w \mathbf{e}, \end{aligned} \tag{6}$$

while (5), (6) yield the rolling condition

$$r_w \dot{\theta}_2 - (r_w + r_b)\dot{\theta}_1 = r_b \dot{\theta}_3. \tag{7}$$

Note that $\dot{\theta}_3$ is not directly measurable. However, for feedback control, $\dot{\theta}_3$ can be obtained from (7) in terms of measurements of $\dot{\theta}_1$ and $\dot{\theta}_2$.

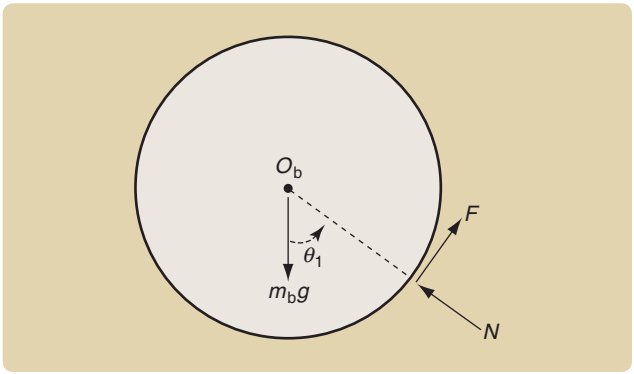


**FIGURE 5** Free-body diagram of the ball. $N$ denotes the normal reaction force due to the wheel, while $F$ denotes the frictional force. The external force $m_b g \cos\theta_1 - N$ provides the centripetal acceleration necessary to keep the ball rolling on the periphery of the wheel.

Using (7), it follows that

$$T = \frac{1}{2} I_w \dot{\theta}_2^2 + \frac{1}{2} m_b (r_w + r_b)^2 \dot{\theta}_1^2 + \frac{1}{5} m_b (r_w \dot{\theta}_2 - r_w \dot{\theta}_1 - r_b \dot{\theta}_1)^2.$$

The total potential energy $V$ is

$$V = m_b g (r_w + r_b) \cos\theta_1,$$

where $g$ is the gravitational acceleration. The Lagrangian function is given by

$$\begin{aligned} L &= T - V \\ &= \frac{1}{2} I_w \dot{\theta}_2^2 + \frac{1}{2} m_b (r_w + r_b)^2 \dot{\theta}_1^2 \\ &\quad + \frac{1}{5} m_b (r_w \dot{\theta}_2 - r_w \dot{\theta}_1 - r_b \dot{\theta}_1)^2 - m_b g (r_w + r_b) \cos\theta_1. \end{aligned}$$

Then, we have

$$\frac{\partial L}{\partial \theta_1} = m_b g (r_w + r_b) \sin\theta_1, \tag{8}$$

$$\begin{aligned} \frac{\partial L}{\partial \dot{\theta}_1} &= \left( \frac{7}{5} r_w^2 m_b + \frac{14}{5} r_w r_b m_b + \frac{7}{5} r_b^2 m_b \right) \dot{\theta}_1 \\ &\quad + \left( -\frac{2}{5} r_w^2 m_b - \frac{2}{5} r_w r_b m_b \right) \dot{\theta}_2, \end{aligned} \tag{9}$$

$$\begin{aligned} \frac{d}{dt}\left( \frac{\partial L}{\partial \dot{\theta}_1} \right) &= \left( \frac{7}{5} r_w^2 m_b + \frac{14}{5} r_w r_b m_b + \frac{7}{5} r_b^2 m_b \right) \ddot{\theta}_1 \\ &\quad + \left( -\frac{2}{5} r_w^2 m_b - \frac{2}{5} r_w r_b m_b \right) \ddot{\theta}_2, \end{aligned} \tag{10}$$

$$\frac{\partial L}{\partial \theta_2(t)} = 0, \tag{11}$$

$$\frac{\partial L}{\partial \dot{\theta}_2} = \left( -\frac{2}{5} r_w^2 m_b - \frac{2}{5} r_w r_b m_b \right) \dot{\theta}_1 + \left( I_w + \frac{2}{5} r_w^2 m_b \right) \dot{\theta}_2, \tag{12}$$

$$\frac{d}{dt}\left( \frac{\partial L}{\partial \dot{\theta}_2} \right) = \left( -\frac{2}{5} r_w^2 m_b - \frac{2}{5} r_w r_b m_b \right) \ddot{\theta}_1 + \left( I_w + \frac{2}{5} r_w^2 m_b \right) \ddot{\theta}_2. \tag{13}$$

From (1) and (8)–(13), the equations of motion are given by

$$(7r_b + 7r_w)\ddot{\theta}_1 - 2r_w \ddot{\theta}_2 - 5g \sin\theta_1 = 0, \tag{14}$$

$$\left( -\frac{2}{5} r_w^2 m_b - \frac{2}{5} r_w r_b m_b \right) \ddot{\theta}_1 + \left( I_w + \frac{2}{5} r_w^2 m_b \right) \ddot{\theta}_2 = \tau. \tag{15}$$

Equations (14) and (15) are valid only when the centripetal force is large enough to maintain the circular motion of the ball on the wheel. Otherwise, the ball can leave the wheel. Consider the free-body diagram of the ball as shown in Figure 5. Using Newton's third law, the force equation for the radial direction is given by

$$m_b g \cos\theta_1 - N = m_b (r_w + r_b) \dot{\theta}_1^2,$$

where $N$ is the normal reaction force. The force provided by $m_b g \cos\theta_1 - N$ is necessary to maintain the circular motion of the ball on the wheel. The ball and the wheel lose contact when $N = 0$, at which time the ball leaves the wheel. Thus, to maintain the ball on the wheel, the condition

$$N = m_b g \cos\theta_1 - m_b (r_w + r_b) \dot{\theta}_1^2 > 0 \tag{16}$$

must be satisfied.

A voltage signal, which is generated according to a control law designed below, is supplied to an amplifier, which drives a permanent magnet dc motor to control the wheel. Since the electrical time constant of a dc motor is usually much smaller than the mechanical time constant, and since the value of the viscous friction coefficient is negligible, the reduced-order dc motor model [29] is given by

$$\tau = \frac{K_m}{R_a} u - \frac{K_m^2}{R_a} \dot{\theta}_2, \tag{17}$$

where $\tau$ is the control torque, $u$ is the control voltage, $K_m$ is the motor constant, and $R_a$ is the motor armature resistance.

The state vector is defined as

$$x = [x_1\ x_2\ x_3\ x_4]^T = [\theta_1\ \dot{\theta}_1\ \theta_2\ \dot{\theta}_2]^T. \tag{18}$$

From (14), (15), and (17), the state-space representation of the ball and wheel system in the basis given by (18) can be written as

$$\dot{x} = f(x) + g(x)u, \tag{19}$$

where

$$f(x) = \begin{bmatrix} x_2 \\ a x_4 + b \sin x_1 \\ x_4 \\ p x_4 + q \sin x_1 \end{bmatrix}, \quad g(x) = \begin{bmatrix} 0 \\ c \\ 0 \\ r \end{bmatrix},$$

and $a$, $b$, $c$, $p$, $q$, $r$ are defined by

$$a = -\frac{2 r_w K_m^2}{R_a (7 I_w + 2 r_w^2 m_b)(r_b + r_w)},$$

$$b = \frac{g(5I_w + 2r_w^2 m_b)}{(7I_w + 2r_w^2 m_b)(r_b + r_w)},$$

$$c = \frac{2r_w K_m}{R_a(7I_w + 2r_w^2 m_b)(r_b + r_w)},$$

$$p = -\frac{7K_m^2}{R_a(7I_w + 2r_w^2 m_b)},$$

$$q = \frac{2gr_w m_b}{7I_w + 2r_w^2 m_b},$$

$$r = \frac{7K_m}{R_a(7I_w + 2r_w^2 m_b)}.$$

Note that

$$ar = cp. \tag{20}$$

## FULL-STATE-FEEDBACK LINEARIZATION

Consider the nonlinear single-input-single-output system (19) and

$$y = h(x), \tag{21}$$

where $x \in \Omega \subset R^n$, $f : \Omega \to R^n$, and $g : \Omega \to R^n$ are smooth vector fields on $\Omega$, $u \in R$ is a scalar control signal, and $h : \Omega \to R$ is a smooth scalar function. The derivative of $h(x)$ along the vector field $f(x)$ is expressed by the *Lie derivative*

$$L_f h(x) = \frac{\partial h}{\partial x} f(x).$$

Intuitively, the Lie derivative of a function $h(x)$ with respect to the vector field $f(x)$ is the rate of change of $h(x)$ along the trajectories of the system $\dot{x} = f(x)$. Note that $L_g L_f h(x) = [\partial(L_f h(x))/\partial x]\, g(x)$, while $L_f^k h(x)$ denotes $L_f(L_f^{k-1} h(x))$, where $L_f^1 h(x) = L_f h(x)$ and $L_f^0 h(x) = h(x)$.

### Definition 1

The system (19), (21) has relative degree $l$ in the region $\Omega$ if

1) $L_g L_f^i h(x) = 0$, $i = 0, 1, \ldots, l-2$ for all $x \in \Omega$.
2) $L_g L_f^{l-1} h(x) \neq 0$ for all $x \in \Omega$.

If the relative degree of the system (19) and (21) is equal to the number of states, then the system is full-state-feedback linearizable by using the change of coordinates

$$\begin{aligned}
\xi_1 &= h(x),\\
\xi_2 &= \dot{\xi}_1 = L_f h(x),\\
\xi_3 &= \dot{\xi}_2 = L_f^2 h(x),\\
&\vdots\\
\xi_n &= \dot{\xi}_{n-1} = L_f^{n-1} h(x),\\
\dot{\xi}_n &= L_f^n h(x) + L_g L_f^{n-1} h(x) u,
\end{aligned}$$

and by choosing the full-state-feedback control

$$u = \frac{1}{L_g L_f^{n-1} h(x)} (v - L_f^n h(x)).$$

The nonlinear system (19) and (21) can then be transformed into a linear time-invariant system in controllable canonical form. Thus, the controller design can be obtained based on the resulting linear form.

It is shown in [5] that the system (19) is full-state-feedback linearizable if and only if there exists an output function $h(x)$ for which the resulting system of the form (19) and (21) has relative degree $n$. Moreover, the existence of the output function $h$ can be characterized by the vector fields $f$ and $g$. To state the conditions of the existence of $h$, the following notions are introduced.

For vector fields $f$ and $g$, the *Lie bracket* $[f, g]$ is defined as

$$[f, g](x) = \frac{\partial g}{\partial x} f(x) - \frac{\partial f}{\partial x} g(x).$$

In compact notation, the Lie bracket is expressed as $ad_f g(x) = [f, g](x)$ and $ad_f^k g(x) = [f, ad_f^{k-1} g](x)$, where $ad_f^1 g(x) = ad_f g(x)$ and $ad_f^0 g(x) = g(x)$. Consider vector fields $f_1, \ldots, f_k$ on $\Omega \subset R^n$. For each $x \in \Omega$, the vectors $f_1(x), \ldots, f_k(x)$ span a subspace of $R^n$, which we denote by

$$\Delta(x) = \text{span}\{f_1(x), \ldots, f_k(x)\}.$$

The collection $\Delta$ of all vector spaces $\Delta(x)$ such that $x \in \Omega$ is called a distribution and is written as

$$\Delta := \bigcup_{x \in \Omega} \Delta(x).$$

The distribution $\Delta$ generated by $f_1, \ldots, f_k$ is denoted by

$$\Delta = \text{span}\{f_1, \ldots, f_k\}.$$

### Definition 2

The distribution $\Delta$ is *involutive* on $\Omega$ if, for all pairs of vector fields $g_1$ and $g_2$ belonging to $\Delta$, the Lie bracket $[g_1, g_2] \in \Delta$.

In [5], it is shown that $\Delta = \text{span}\{f_1, \ldots, f_k\}$ is involutive on $\Omega$ if and only if

$$[f_i, f_j] \in \Delta, \text{ for all } 1 \leq i, j \leq k. \tag{22}$$

A distribution $\Delta = \text{span}\{f_1, \ldots, f_k\}$, defined on $\Omega \subset R^n$, is *nonsingular* if

$$\dim(\Delta(x)) = k$$

for all $x \in \Omega$.

### Definition 3

The nonsingular distribution $\Delta$, defined on $\Omega \subset R^n$, is *completely integrable* if, for each point $x_0 \in \Omega$, there exists a neighborhood $\Omega_0$ of $x_0$ and $n - k$ real-valued smooth functions $h_1(x), \ldots, h_{n-k}(x)$, all defined on $\Omega_0$, such that

$$\frac{\partial h_j}{\partial x} f_i(x) = 0, \text{ for all } 1 \leq i \leq k \text{ and } 1 \leq j \leq n - k, \tag{23}$$

and such that the row vectors $(\partial h_1/\partial x), \ldots, (\partial h_{n-k}/\partial x)$ are linearly independent.

The following theorem gives necessary and sufficient conditions for complete integrability. For details, see [5].

### Theorem 1

A nonsingular distribution is completely integrable if and only if it is involutive.

Necessary and sufficient conditions for feedback linearizability of system (19) are given in the following theorem. For details, see [5]–[7].

### Theorem 2

The nonlinear system (19) is full-state-feedback linearizable if and only if there exists a domain $\Omega \subset R^n$ such that the following conditions hold:

1) The matrix $G(x) = [g(x), ad_f g(x), \ldots, ad_f^{n-1} g(x)]$ has rank $n$ for all $x \in \Omega$.
2) The distribution $\Delta = \text{span}\{g, ad_f g, \ldots, ad_f^{n-2} g\}$ is involutive on $\Omega$.

## STABILIZATION BASED ON FULL-STATE-FEEDBACK LINEARIZATION

To show that the ball and wheel system is full-state-feedback linearizable, we consider the necessary and sufficient conditions for feedback linearizability given by Theorem 2. Computing $ad_f g(x)$, $ad_f^2 g(x)$, and $ad_f^3 g(x)$ yields

$$ad_f g(x) = \begin{bmatrix} -c \\ -ar \\ -r \\ -pr \end{bmatrix},$$

$$ad_f^2 g(x) = \begin{bmatrix} ar \\ bc\cos x_1 + apr \\ pr \\ cq\cos x_1 + p^2 r \end{bmatrix},$$

$$ad_f^3 g(x) = \begin{bmatrix} -bc\cos x_1 - apr \\ -bcx_2 \sin x_1 - abr\cos x_1 - acq\cos x_1 - ap^2 r \\ -cq\cos x_1 - p^2 r \\ -cqx_2 \sin x_1 - aqr\cos x_1 - cpr\cos x_1 - p^3 r \end{bmatrix}.$$

The determinant of $G(x)$ is thus given by

$$\begin{aligned} \det(G(x)) &= \det[g(x), ad_f g(x), ad_f^2 g(x), ad_f^3 g(x)] \\ &= (c^4 q^2 - 2bc^3 qr + b^2 c^2 r^2)(\cos x_1)^2 \\ &= \frac{400 g^2 K_m^4 r_w^2}{(7I_w + 2r_w^2 m_b)^4 (r_b + r_w)^4 R_a^4}(\cos x_1)^2, \end{aligned}$$

which is positive for all $x_1 \in (-(\pi/2), (\pi/2))$. Hence $G(x)$ is full rank in $\Omega$, where

$$\Omega = \left\{ x \in R^4 \,|\, -\frac{\pi}{2} < x_1 < \frac{\pi}{2} \right\}. \tag{24}$$

Thus, condition (1) of Theorem 2 is satisfied for $\Omega$ given by (24). Denote

$$\Delta = \text{span}\{g, ad_f g, ad_f^2 g\}.$$

Using (22) to show that $\Delta$ is involutive in $\Omega$, we need to show that $[g(x), ad_f g(x)]$, $[g(x), ad_f^2 g(x)]$, and $[ad_f g(x), ad_f^2 g(x)]$ are in $\Delta$. By computing $[g(x), ad_f g(x)]$, $[g(x), ad_f^2 g(x)]$, and $[ad_f g(x), ad_f^2 g(x)]$, we obtain

$$\begin{aligned} [g(x), ad_f\, g(x)] &= [0\ 0\ 0\ 0]^T, \\ [g(x), ad_f^2 g(x)] &= [0\ 0\ 0\ 0]^T, \\ [ad_f g(x), \ ad_f^2\, g(x)] &= \begin{bmatrix} 0 \\ -bc^2 \sin x_1 \\ 0 \\ -c^2 q \sin x_1 \end{bmatrix}. \end{aligned}$$

Note that $[g(x), ad_f g(x)]$ and $[g(x), ad_f^2 g(x)]$ are in $\Delta$. Also, using (20), it follows that

$$[ad_f g(x), ad_f^2 g(x)] = -cp(\tan x_1) ad_f g(x) - c(\tan x_1) ad_f^2 g(x).$$

Hence the distribution $\Delta$ is involutive in $\Omega$. The system is therefore full-state-feedback linearizable in $\Omega$. Since $g(x)$, $ad_f g(x)$, and $ad_f^2 g(x)$ are linearly independent, the distribution $\Delta$ is nonsingular. Then, by Theorem 1, the distribution $\Delta$ is completely integrable, and there exists an output function $h(x)$ satisfying the partial differential equations (23) of the Frobenius type

$$L_g h(x) = 0, \tag{25}$$
$$L_{ad_f g} h(x) = 0, \tag{26}$$
$$L_{ad_f^2 g} h(x) = 0, \tag{27}$$
$$L_{ad_f^3 g} h(x) \neq 0. \tag{28}$$

Note that (28) holds because $g(x)$, $ad_f g(x)$, $ad_f^2 g(x)$, and $ad_f^3 g(x)$ are linearly independent. The partial differential equations (25)–(28) are equivalent to the conditions for which the system has relative degree four in $\Omega$

$$L_g h(x) = 0, \tag{29}$$
$$L_g L_f h(x) = 0, \tag{30}$$
$$L_g L_f^2 h(x) = 0, \tag{31}$$
$$L_g L_f^3 h(x) \neq 0. \tag{32}$$

A solution to the partial differential equations (25)–(28) is given by

$$y = h(x) = rx_1 - cx_3.$$

The change of variables

$$\xi_1 = h(x) = rx_1 - cx_3, \tag{33}$$
$$\xi_2 = L_f h(x) = rx_2 - cx_4, \tag{34}$$
$$\xi_3 = L_f^2 h(x) = (br - cq)\sin x_1, \tag{35}$$
$$\xi_4 = L_f^3 h(x) = (br - cq)x_2 \cos x_1, \tag{36}$$

transforms the system (19) into

$$\begin{aligned}\dot{\xi}_1 &= \xi_2,\\ \dot{\xi}_2 &= \xi_3,\\ \dot{\xi}_3 &= \xi_4,\\ \dot{\xi}_4 &= L_f^4 h(x) + L_g L_f^3 h(x)\, u,\end{aligned}$$

where

$$\begin{aligned}L_f^4 h(x) = &-(br - cq)x_2^2 \sin x_1\\ &+ (br - cq)(ax_4 + b \sin x_1)\cos x_1,\\ L_g L_f^3 h(x) = &\, c(br - cq)\cos x_1.\end{aligned}$$

In terms of physical parameters, we have

$$L_g L_f^3 h(x) = \frac{10 r_w K_m^2 g}{R_a^2(7I_w + 2r_w^2 m_b)^2(r_w + r_b)^2}\cos x_1,$$

which is nonzero in $\Omega$. Then, the state feedback control

$$u = \frac{1}{L_g L_f^3 h(x)}[v - L_f^4 h(x)] \tag{37}$$

results in the controllable linear system

$$\dot{\xi}_1 = \xi_2, \tag{38}$$
$$\dot{\xi}_2 = \xi_3, \tag{39}$$
$$\dot{\xi}_3 = \xi_4, \tag{40}$$
$$\dot{\xi}_4 = v. \tag{41}$$

For stabilization, the new control variable $v$ introduced in (37) and appearing in (41) is then taken as a linear feedback control

$$v = -K_1\xi_1 - K_2\xi_2 - K_3\xi_3 - K_4\xi_4, \tag{42}$$

where the linear feedback gain matrix $[K_1\, K_2\, K_3\, K_4]$ can be determined by using a pole-placement method to place the closed-loop poles in the open left-half plane. The designed controller establishes asymptotic stability in the region $\Omega = \{[\theta_1\ \dot{\theta}_1\ \theta_2\ \dot{\theta}_2]^T \in R^4 \,|\, |\theta_1| < \pi/2\}$. However, from (37) it is clear that a sufficiently large angular position of the ball can result in saturation of the control voltage, which may give rise to closed-loop instability. Thus, due to the limitation on the available input torque from the motor, the actual region of attraction is smaller than $\Omega$. Furthermore, the process of controller design does not take the constraint (16) into account. In fact, it can be seen from (16) that a sufficiently large angular position of the ball can result in the ball leaving the wheel. Hence, the region of attraction also depends on the constraint (16).

Since linearization by state feedback involves exact cancellation of nonlinear terms, the cancellation is not exact in practice due to model uncertainty and measurement error, and thus the resulting closed-loop system may exhibit undesirable behavior. Techniques are given in [7], [30], and [31] for designing robust feedback linearization controllers.

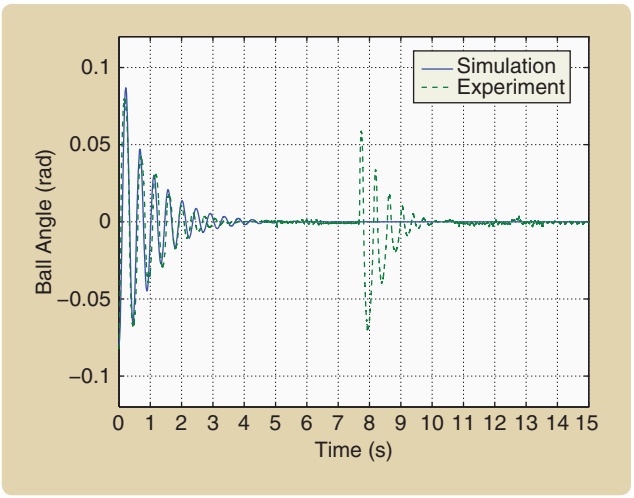


**FIGURE 6** A comparison of simulation and experimental results of the angular position response of the ball. The initial conditions are $\theta_1(0) = -0.08$ rad, $\dot{\theta}_1(0) = 0$ rad/s, $\theta_2(0) = 0.08$ rad, and $\dot{\theta}_2(0) = 0$ rad/s. Both simulation and experimental results show that the angular position of the ball converges to zero. At time 7.6 s, an impulsive disturbance is introduced in the experiment by tapping the ball. The system subsequently recovers from this velocity perturbation.

## SIMULATION AND EXPERIMENTAL RESULTS

To observe the performance of the control law (37) and (42), the control system is simulated in Matlab/Simulink using the parameters in Table 1. The closed-loop poles are chosen to be $\{-1 \pm \jmath 14, -2 \pm \jmath 2.5\}$, which corresponds to the control gain $[K_1\, K_2\, K_3\, K_4] = [2019.25 \quad 808.5 \quad 215.25 \quad 6]$. The designed control algorithm is tested on the experimental setup as shown in Figure 1 and executed on the DSP system written in C. The sampling frequency of the system is chosen to be 1 kHz. The initial conditions are set to $\theta_1(0) = -0.08$ rad $(-4.5837°)$, $\dot{\theta}_1(0) = 0$ rad/s, $\theta_2(0) = 0.08$ rad $(4.5837°)$, and $\dot{\theta}_2(0) = 0$ rad/s.

The simulation and experimental results of the angular position response of the ball, the angular position response of the wheel, and the control voltage are shown in figures 6, 7, and 8, respectively. As can be seen in figures 6 and 7, both simulation and experimental results confirm that the controller (37) and (42) stabilizes the system. To examine the performance of the control system with different initial conditions, after the system converges to the equilibrium, an impulsive disturbance is added manually by pushing the ball away from the equilibrium state to give a nonzero initial velocity. From the experimental results shown in figures 6 and 7, it can be seen that the system converges to the equilibrium from the perturbed state.

The operating range of the control voltage, which is $\pm 20$ V, is constrained by the motor driver. From Figure 8,

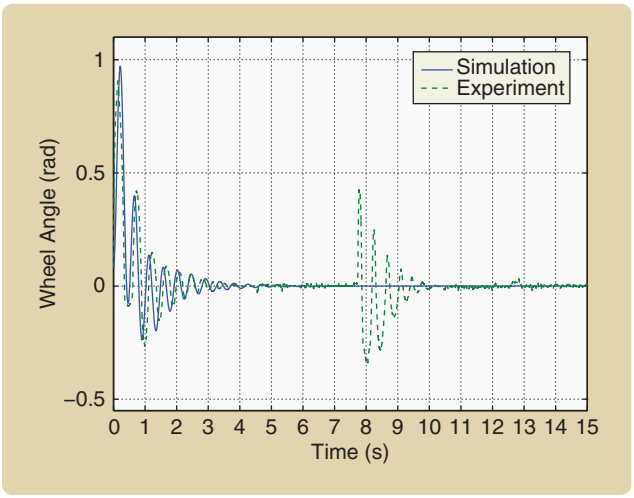


**FIGURE 7** A comparison of simulation and experimental results of the angular position response of the wheel. The initial conditions are $\theta_1(0) = -0.08$ rad, $\dot{\theta}_1(0) = 0$ rad/s, $\theta_2(0) = 0.08$ rad, and $\dot{\theta}_2(0) = 0$ rad/s. The motor rotates the wheel to bring the ball to the equilibrium. The oscillation at time 7.6 s is the response to the impulsive disturbance induced in the experiment by tapping the ball.

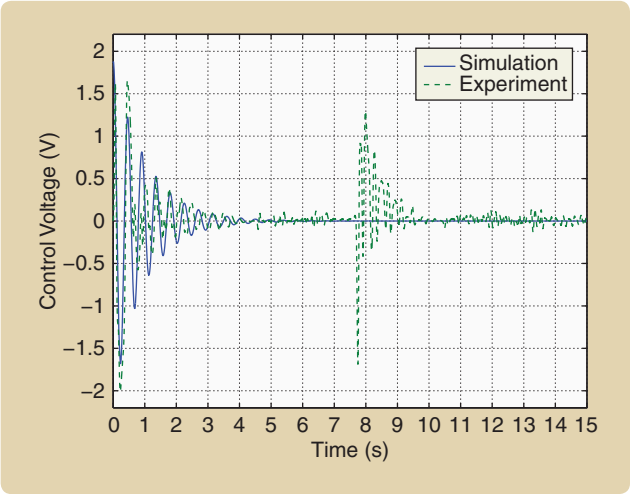


**FIGURE 8** A comparison of simulation and experimental results of the control voltage. The operating range of the control voltage is $\pm 20$ V, which is constrained by the motor driver. The control voltages are not saturated in either the simulation or the experiment.

the control voltages are not saturated in either simulation or experiment for the chosen initial conditions. As discussed in the previous section, a sufficiently large initial angular position of the ball can result in saturation of the control voltage and reduce the region of attraction. By simulation, the control voltage becomes saturated when $\theta_1(0)$ reaches 0.7505 rad $(43.022°)$ with $[\dot{\theta}_1(0)\ \theta_2(0)\ \dot{\theta}_2(0)] = [0\ 0\ 0]$. By comparing the simulation results with the experimental results shown in figures 6, 7, and 8, the maximum differences between the simulated and measured angular position of the ball, angular position of the wheel, and control

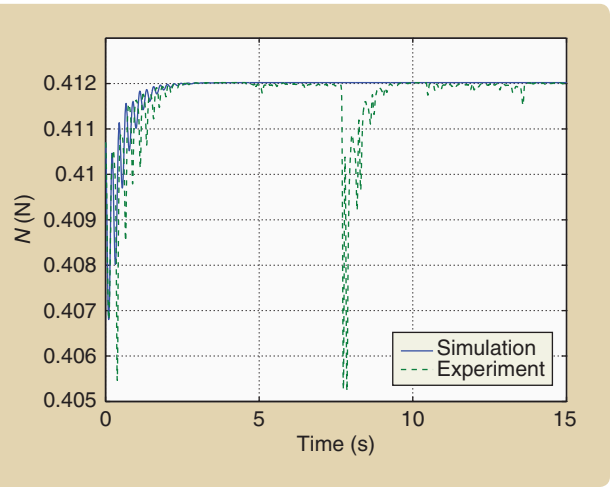


**FIGURE 9** Simulation and experimental results for the response of the normal force $N$ in Newtons. The initial conditions are $\theta_1(0) = -0.08$ rad, $\dot{\theta}_1(0) = 0$ rad/s, $\theta_2(0) = 0.08$ rad, and $\dot{\theta}_2(0) = 0$ rad/s. Since $N$ remains positive for all time, the ball does not leave the wheel.

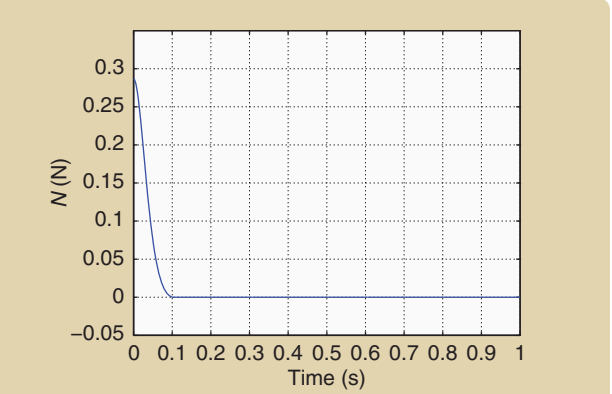


**FIGURE 10** Simulation result of the response of $N$. To verify that a sufficiently large initial angular position of the ball can result in the ball leaving the wheel, the initial condition is chosen to be $[\theta_1(0)\ \dot{\theta}_1(0)\ \theta_2(0)\ \dot{\theta}_2(0)] = [0.8 \text{ rad } 0\ 0\ 0]$. Note that $N = 0$ at time 0.1 s, at which time the simulated ball separates from the wheel and $N$ remains zero.

voltage are $6.96 \times 10^{-3}$ rad $(0.3988°)$, 0.0644 rad $(3.69°)$, and 0.457 V, respectively. The slight mismatch between simulation and experimental results is possibly caused by disturbances and unmodeled hardware effects. In Figure 9, both simulation and experimental results show that the constraint (16) is satisfied, and thus the ball remains on the wheel during the experiment. By simulation, Figure 10 shows that the ball leaves the wheel when $\theta_1(0)$ reaches 0.8 rad $(45.837°)$ with $[\dot{\theta}_1(0)\ \theta_2(0)\ \dot{\theta}_2(0)] = [0\ 0\ 0]$. In practice, due to the friction between the ball and the wheel, the actual region in which the ball can be stabilized by the control law is much smaller. From the experiment, the ball is no longer stabilizable when $|\theta_1(0)| > 0.2617$ rad $(15°)$ with $[\dot{\theta}_1(0)\ \theta_2(0)\ \dot{\theta}_2(0)] = [0\ 0\ 0]$.

## CONCLUSIONS

In this article, the ball and wheel system was considered. A mathematical model of the system was derived to facilitate the controller design. It was shown that this system is locally full-state-feedback linearizable, and a stabilizing control law was obtained based on full-state-feedback linearization. The experimental apparatus was constructed, and the controller was implemented. Simulation and experimental results were presented to demonstrate the effectiveness of the designed controller. This experimental device is easy to build, inexpensive, and well suited for nonlinear control study.


## ACKNOWLEDGMENTS

This work was supported by the National Science Council of Taiwan under Grant NSC 95-2221-E-006-366.


## AUTHOR INFORMATION


***Ming-Tzu Ho*** (bruceho@mail.ncku.edu.tw) received the B.S. degree in engineering science from National Cheng Kung University, Taiwan, in 1988, and the M.S. and Ph.D. degrees in electrical engineering from Texas A&M University, College Station, in 1993 and 1997, respectively. From 1998 to 1999, he was a researcher at Ritek Corporation, Taiwan, where he worked on control and system integration of CD and DVD mastering systems. Since 1999, he has been with the Department of Engineering Science at National Cheng Kung University, Taiwan, where he is currently an associate professor. His research interests include nonlinear control, robust control, PID control, and control applications. He is a coauthor of *Structure and Synthesis of PID Controllers* (Springer-Verlag, 2000). He can be contacted at the Department of Engineering Science, National Cheng Kung University, Tainan 701, Taiwan.

***Yi-Wei Tu*** received the B.S. degree in electrical engineering from the Southern Taiwan University of Technology, Taiwan, in 2003. He is currently a Ph.D. candidate in the Department of Engineering Science of the National Cheng Kung University, Taiwan. His research interests include control theory and applications, digital signal processing, and image processing.

***Hao-Shuan Lin*** obtained the B.S. degree in electrical engineering from Kun Shan University, Taiwan, in 2004, and the M.S. degree in engineering science from National Cheng Kung University, Taiwan, in 2006.


## REFERENCES


[1] S. Mori, H. Nishihara, and K. Furuta, "Control of unstable mechanical system: Control of pendulum," *Int. J. Control*, vol. 23, no. 5, pp. 673–692, 1976.

[2] K. Furuta, M. Yamakita, S. Kobayashi, and M. Nishimura, "A new inverted pendulum apparatus for education," in *Proc. IFAC Symp. Advances in Control Education*, Boston, MA, 1994, pp. 191–196.

[3] J. Hauser, S. Sastry, and P. Kokotovic, "Nonlinear control via approximate input-output: The ball and beam example," *IEEE Trans. Automat. Control*, vol. 37, no. 3, pp. 392–398, 1992.

[4] M. L. Moore, J. T. Musacchio, and K. M. Passino, "Genetic adaptive control for an inverted wedge: Experiments and comparative analyses," *Eng. Appl. Artif. Intell.*, vol. 14, no. 1, pp. 1–14, 2001.

[5] A. Isidori, *Nonlinear Control Systems*. London: Springer-Verlag, 1995.

[6] H. Nijmeijer and A. J. Van der Schaft, *Nonlinear Dynamical Control Systems*. New York: Springer-Verlag, 1990.

[7] R. Marino and P. Tomei, *Nonlinear Control Design: Geometric, Adaptive and Robust*. London: Prentice Hall, 1995.

[8] M. Bodson, J. Chiasson, and R. Novotnak, "High-performance induction motor control via input-output linearization," *IEEE Control Syst. Mag.*, vol. 14, no. 4, pp. 25–33, 1994.

[9] L. Guzzella and A. M. Schmid, "Feedback linearization of spark-ignition engines with continuously variable transmissions," *IEEE Trans. Control Syst. Technol.*, vol. 3, no. 1, pp. 54–60, 1995.

[10] L. Del Re and A. Isidori, "Performance enhancement of nonlinear drives by feedback linearization of linear-bilinear cascade models," *IEEE Trans. Control Syst. Technol.*, vol. 3, no. 3, pp. 299–308, 1995.

[11] S. N. Singh and W. Yim, "Feedback linearization and solar pressure satellite attitude control," *IEEE Trans. Aerospace Electron. Syst.*, vol. 32, no. 2, pp. 732–741, 1996.

[12] O. Akhrif, F. A. Okou, L. A. Dessaint, and R. Champagne, "Application of a multivariable feedback linearization scheme for rotor angle stability and voltage regulation of power systems," *IEEE Trans. Power Syst.*, vol. 14, no. 2, pp. 620–628, 1999.

[13] H. D. Lee, S. J. Kang, and S. K. Sul, "Efficiency-optimized direct torque control of synchronous reluctance motor using feedback linearization," *IEEE Trans. Ind. Electron.*, vol. 46, no. 1, pp. 192–198, 1999.

[14] D. C. Lee, G. M. Lee, and K. D. Lee, "DC-bus voltage control of three-phase AC/DC PWM converters using feedback linearization," *IEEE Trans. Ind. Appl.*, vol. 36, no. 3, pp. 826–833, 2000.

[15] J. D. Lindlau and C. R. Knospe, "Feedback linearization of an active magnetic bearing with voltage control," *IEEE Trans. Control Syst. Technol.*, vol. 10, no. 1, pp. 21–31, 2002.

[16] M. Chen and C. R. Knospe, "Feedback linearization of active magnetic bearings: current-mode implementation," *IEEE/ASME Trans. Mechatron.*, vol. 10, no. 6, pp. 632–639, 2005.

[17] A. E. Hajjaji and M. Ouladsine, "Modeling and nonlinear control of magnetic levitation systems," *IEEE Trans. Ind. Electron.*, vol. 48, no. 4, pp. 831–838, 2001.

[18] M. Spong, P. Corke, and R. Lozano, "Nonlinear control of the inertia wheel pendulum," *Automatica*, vol. 37, pp. 1845–1851, 2001.

[19] M. Bodson, J. N. Chiasson, R. T. Novotnak, and R. B. Rekowski, "High-performance nonlinear feedback control of a permanent magnet stepper motor," *IEEE Trans. Control Syst. Technol.*, vol. 1, no. 1, pp. 5–14, 1993.

[20] J. Chiasson and M. Bodson, "Nonlinear control of a shunt DC motor," *IEEE Trans. Automat. Control*, vol. 38, no. 11, pp. 1662–1666, 1993.

[21] B. Grcar, P. Cafuta, M. Znidaric, and F. Gausch, "Backstepping dynamic compensator design for the PMAC servo-drive," *IEEE Trans. Energy Conversion*, vol. 14, no. 4, pp. 1396–1401, 1999.

[22] J. Solsona, M. I. Valla, and C. Muravchik, "Nonlinear control of a permanent magnet synchronous motor with disturbance torque estimation," *IEEE Trans. Energy Conversion*, vol. 15, no. 2, pp. 163–168, 2000.

[23] J. Chiasson, "A new approach to dynamic feedback linearization control of an induction motor," *IEEE Trans. Automat. Control*, vol. 43, no. 3, pp. 391–397, 1998.

[24] T. K. Boukas and T. G. Habetler, "High-performance induction motor speed control using exact feedback linearization with state and state derivative feedback," *IEEE Trans. Power Electron.*, vol. 19, no. 4, pp. 1022–1028, 2004.

[25] S. Fuchshumer, K. Schlacher, M. Pölzer, and G. Grabmair, "Flatness based control of the system 'ball on the wheel'," in *Proc. 6th IFAC Symp. Nonlinear Control Systems*, Stuttgart, Germany, 2004, pp. 227–232.

[26] Movie ball on wheel. [Online]. Available: http://regpro.mechatronik.uni-linz.ac.at/education/diplomas/mastersgallery/ballonwheel/

[27] M. T. Ho and J. M. Lu, "$H_\infty$ PID controller design for Luré systems and its application to a ball and wheel apparatus," *Int. J. Control*, vol. 78, no. 1, pp. 53–64, 2005.

[28] H. Goldstein, C. Poole, and J. Safko, *Classical Mechanics*. Upper Saddle River, NJ: Addison Wesley, 2002.

[29] V. Utkin, J. Guldner, and J. Shi, *Sliding Mode Control in Electromechanical Systems*. Boca Raton, FL: CRC Press, 1999.

[30] J. J. Slotine and K. Hedrick, "Robust input-output feedback linearization," *Int. J. Control*, vol. 57, no. 5, pp. 1133–1139, 1993.

[31] A. D. Franco, H. Bourlès, E. R. Pieri, and H. Guillard, "Robust nonlinear control associating robust feedback linearization and control," *IEEE Trans. Automat. Control*, vol. 51, no. 7, pp. 1200–1207, 2006.